*Journal of Sound and Vibration* (2000) **234**(1), 43–66
doi:10.1006/jsvi.1999.2853, available online at http://www.idealibrary.com on IDEAL®

# SURFACE GROUND VIBRATION DUE TO A MOVING TRAIN IN A TUNNEL: TWO-DIMENSIONAL MODEL

A. V. Metrikine and A. C. W. M. Vrouwenvelder

*Faculty of Civil Engineering and Geosciences, Delft University of Technology, Stevinweg* 1, 2628 *CN Delft, Netherlands*

(*Received* 23 *August* 1999, *and in final form* 29 *November* 1999)

Vibration of a surface of a two-dimensional (2D) elastic layer generated by a point load moving uniformly along a beam, which is located inside the layer is investigated theoretically. It is supposed that the layer possesses a small viscosity, is fixed along the bottom, and has a traction-free surface. The beam is described by the Euler–Bernoulli model and located parallel both to the surface and the bottom of the layer. The surface vibration is analysed under three types of the load, namely constant, harmonically varying and a stationary random load. For the deterministic loads, the vector displacement of an observation point on the layer surface is analyzed along with the amplitude spectrum of vibration in this point. For the random load main attention is paid to the variance of vibration at the observation point. Qualitative features of obtained results are discussed via kinematic analyses of the wave propagation in the structure.



## 1. INTRODUCTION

It is well known that vibrations produced by a moving train can propagate in the ground and be perceptible at significant distances [1]. As recently reported in references [2–5], the level of these vibrations increases if trains run at high speeds close to the minimal phase velocity of the track-ground structure, which is normally about the Rayleigh wave velocity [6, 7]. In a soft (peat) ground, this velocity is of the order of 200 km/h or even smaller and can be simply exceeded by currently operating high-speed trains. Therefore, the research on vibrations caused by trains is of indubitable practical importance.

In this paper, vibrations of a ground surface due to a moving train in a tunnel are theoretically considered. At train speed about 200 km/h these vibrations can be quite powerful (about 10 mm), though they are excited relatively deep in the ground. Due to this fact, before letting a train move in a tunnel with a high speed one has to estimate the level of the surface ground vibration.

The new academic element of our study in comparison to works presented in references [2–7] is that the vibrations are now excited by a load moving inside the ground and the energy is transferred to an observation point on the surface by only the bulk waves. This is in contrast to the case of the load motion over the surface, when the vibrations are primarily transmitted by the Rayleigh waves.

To estimate the level of the ground vibrations a relatively simple two-dimensional model is considered, which consists of an elastic layer, possessing a small viscosity, and a beam locating inside the layer. It is assumed that the layer is infinitely long in the horizontal direction, is fixed along the bottom and its surface is traction-free. The beam is considered infinitely long, described by the Euler–Bernoulli model and located parallel to both the surface and the bottom of the layer.

0022-460X/00/260043 + 24 $35.00/0 

Motion of the structure is caused by a point load $P(t)$, which moves uniformly along the beam. Three types of the load $P(t)$ are investigated in the paper, namely constant, a harmonically varying and a stationary random load. The constant load represents the pressure on the rails a train produces due to the gravity force. By means of the harmonically varying load distinguished frequencies of the loading spectrum are taken into account. These frequencies may be related, for example, to the whole-wagon vibrations, to non-roundness of the train wheels or to the sleeper-passing frequency. The assumption about the randomness of the load is the most general one. It allows considering a wide spectrum of the loading force, one faces in reality.

All three types of considered loading processes, after a substantially long time, lead to the stationary vibrations in the reference system moving with the load. Due to this fact, it is adequate to apply the integral Fourier transforms for the mathematical analysis of the problem. By employing these transforms in Section 3, general expressions are obtained for the vector displacement of an observation point on the layer surface and for the amplitude spectrum of this displacement.

In section 4 an analysis is performed of the dispersion of waves in the structure, which serves as a basis for the further study. Sections 5–7 are concerned with the structural response to constant, harmonic and random loads, respectively. For the deterministic loads considered in sections 5 and 6, the displacements and the amplitude spectrum of vibrations in the observation point are analyzed. A physical interpretation of the results obtained is given by employing the kinematic analysis of the wave propagation in the structure. For the random load studied in section 7, main attention is paid to the variance of vibrations in the observation point. In all sections, the effect of the load velocity on the structural response is carefully discussed.

## 2. MODEL AND GOVERNING EQUATIONS

The model under consideration is composed of a two-dimensional layer, a beam and a uniformly moving load as depicted in Figure 1. The layer has a thickness $(h + H)$ in the $z$ direction. The beam is aligned in the $x$ direction and located at distance $h$ from the layer surface. The vertical point load $P(t)$ acts upon the beam at the point $x = Vt$.

Taking into account a small viscosity in the layer, one may write the equation of its motion as [8]

$$\hat{\mu}\nabla_{x,z}^2\mathbf{u} + (\hat{\lambda} + \hat{\mu})\,\nabla_{x,z}(\nabla_{x,z}\,\mathbf{u}) = \rho\,\frac{\partial^2\mathbf{u}}{\partial t^2}, \tag{1}$$

where $\mathbf{u}(x, z, t) = \{u(x, z, t), w(x, z, t)\}$ is the vector displacement, $\rho$ is the mass density of the layer, $\hat{\lambda} = \lambda + \lambda^* \partial/\partial t$ and $\hat{\mu} = \mu + \mu^* \partial/\partial t$ are operators used instead of Lamé constants $\lambda$ and $\mu$ to describe the visco-elastic behaviour of the layer.

The equation of the beam vertical motion reads

$$\rho_B\,\frac{\partial^2 W}{\partial t^2} + EI\,\frac{\partial^4 W}{\partial x^4} = P(t)\delta(x - Vt) + a(\sigma_{zz}(x, h - 0, t) - \sigma_{zz}(x, h + 0t)), \tag{2}$$

where $\sigma_{zz}(x, z)$ is the vertical stress, $W(x, t)$ is the beam vertical displacement, $\rho_B$ and $EI$ are the mass per unit length and the bending stiffness of the beam, $\delta(\cdots)$ is the Dirac delta function, and $a$ is a characteristic length associated with the length of the structure in the $y$ direction.

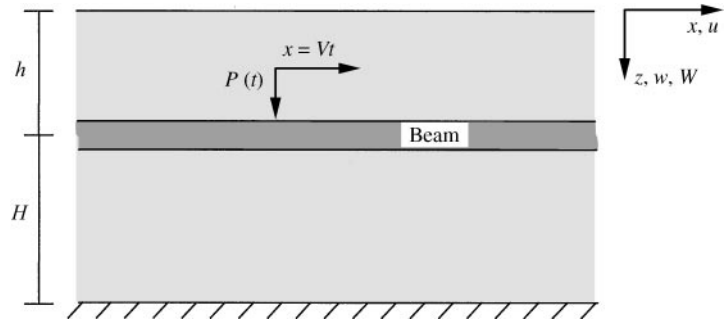


Figure 1. Model.

It is assumed that the beam does not move horizontally and the beam and the layer displacements are equal at the interfaces $z = h \pm 0$. This leads to the following interface conditions:

$$u(x, h + 0, t) = u(x, h - 0, t) = 0, \quad w(x, h + 0, t) = w(x, h - 0, t) = W(x, t). \tag{3}$$

Adding the boundary conditions at $z = 0$ and $h + H$ given as

$$\sigma_{zz}(x, 0, t) = \sigma_{zz}(x, 0, t) = 0, \quad u(x, h + H, t) = w(x, h + H, t) = 0 \tag{4}$$

complete the problem statement.

## 3. SOLUTION OF THE PROBLEM IN GENERAL FORM

It is customary to describe the layer motion in terms of the Lamé potentials taken in the form

$$\phi = \phi(x, z, t), \quad \mathbf{H} = (0, -\psi(x, z, t), 0).$$

The displacement and the stress components in this case are

$$u = \frac{\partial \phi}{\partial x} + \frac{\partial \psi}{\partial z}, \qquad w = \frac{\partial \phi}{\partial z} - \frac{\partial \psi}{\partial x}, \tag{5}$$

$$\sigma_{zz} = \hat{\lambda}\left(\frac{\partial^2 \phi}{\partial x^2} + \frac{\partial^2 \phi}{\partial z^2}\right) + 2\hat{\mu}\left(\frac{\partial^2 \phi}{\partial z^2} - \frac{\partial^2 \psi}{\partial x \partial z}\right), \quad \sigma_{zz} = \hat{\mu}\left(2\frac{\partial^2 \phi}{\partial x \partial z} - \frac{\partial^2 \psi}{\partial x^2} + \frac{\partial^2 \psi}{\partial z^2}\right), \tag{6}$$

and equation (1) splits into following two equations:

$$\frac{\partial^2 \phi}{\partial t^2} - \left(c_L^2 + \frac{\lambda^* + 2\mu^*}{\rho}\frac{\partial}{\partial t}\right)\left(\frac{\partial^2 \phi}{\partial x^2} + \frac{\partial^2 \phi}{\partial z^2}\right) = 0, \tag{7}$$

$$\frac{\partial^2 \psi}{\partial t^2} - \left(c_T^2 + \frac{\mu^*}{\rho}\frac{\partial}{\partial t}\right)\left(\frac{\partial^2 \psi}{\partial x^2} + \frac{\partial^2 \psi}{\partial z^2}\right) = 0, \tag{8}$$

where $c_L = \sqrt{(\lambda + 2\mu)/\rho}$ and $c_T = \sqrt{\mu/\rho}$ are velocities of the compressional and the shear waves in the layer.

To find the steady state response of the system, integral Fourier transforms with respect to time and co-ordinate $x$ are applied. Denoting the Fourier images by double tildes and defining these transforms as

$$\tilde{\tilde{f}}(k,\omega)=\int_{-\infty}^{+\infty}\int_{-\infty}^{+\infty} f(x,t)\exp(\mathrm{i}(\omega t-kx))\,\mathrm{d}x\mathrm{d}t,\quad f(x,t)=\frac{1}{2\pi}\int_{-\infty}^{+\infty}\int_{-\infty}^{+\infty}\tilde{\tilde{f}}(k,\omega)\exp(-\mathrm{i}(\omega t-kx))\mathrm{d}x\mathrm{d}t,$$

one obtains:

- for the layer motion (from equations (7) and (8),

$$-\omega^2\tilde{\tilde{\phi}}-\left(c_L^2-i\omega\frac{\lambda^*+2\mu^*}{\rho}\right)\left(-k^2\tilde{\tilde{\phi}}+\frac{\partial^2\tilde{\tilde{\phi}}}{\partial z^2}\right)=0, \tag{9}$$

$$-\omega^2\tilde{\tilde{\psi}}-\left(c_T^2-i\omega\frac{\mu^*}{\rho}\right)\left(-k^2\tilde{\tilde{\psi}}+\frac{\partial^2\tilde{\tilde{\psi}}}{\partial z^2}\right)=0; \tag{10}$$

- for the beam motion (from equation (2)),

$$\tilde{\tilde{w}}(k,\omega)(EI\,k^4-\rho_B\omega^2)=\tilde{P}(\omega-kV)+a(\tilde{\tilde{\sigma}}_{zz}(k,h-0,\omega)-\tilde{\tilde{\sigma}}_{zz}(k,h+0,\omega)), \tag{11}$$

where

$$\tilde{P}(\omega)=\int_{-\infty}^{+\infty}P(t)\exp(\mathrm{i}\omega t)\,\mathrm{d}t;$$

- for the interface conditions (from equation (3)),

$$\tilde{\tilde{u}}(k,h+0,\omega)=\tilde{\tilde{u}}(k,h-0,\omega)=0,\quad \tilde{\tilde{w}}(k,h+0,\omega)=\tilde{\tilde{w}}(k,\ h-0,\omega)=\tilde{\tilde{W}}(k,\omega); \tag{12}$$

- for the boundary conditions (from equation (4)),

$$\tilde{\tilde{\sigma}}_{zz}(k,0,\omega)=\tilde{\tilde{\sigma}}_{xz}(k,0,\omega)=0,\quad \tilde{\tilde{u}}(k,h+H,\omega)=\tilde{\tilde{w}}(k,h+H,\omega)=0, \tag{13}$$

where, in accordance with expressions (5) and (6)

$$\tilde{\tilde{u}}(k,z,\omega)=\mathrm{i}k\tilde{\tilde{\phi}}+\frac{\partial\tilde{\tilde{\psi}}}{\partial z},\quad \tilde{\tilde{w}}(k,z,\omega)=\frac{\partial\tilde{\tilde{\phi}}}{\partial z}-\mathrm{i}k\tilde{\tilde{\psi}}, \tag{14}$$

$$\tilde{\tilde{\sigma}}_{zz}(k,z,\omega)=(\lambda-\mathrm{i}\omega\lambda^*)\left(-k^2\tilde{\tilde{\phi}}+\frac{\partial^2\tilde{\tilde{\phi}}}{\partial z^2}\right)+2(\mu-\mathrm{i}\omega\mu^*)\left(\frac{\partial^2\tilde{\tilde{\phi}}}{\partial z^2}-\mathrm{i}k\frac{\partial\tilde{\tilde{\psi}}}{\partial z}\right), \tag{15}$$

$$\tilde{\tilde{\sigma}}_{xz}(k,z,\omega)=2\mathrm{i}k\frac{\partial\tilde{\tilde{\phi}}}{\partial z}+k^2\tilde{\tilde{\psi}}+\frac{\partial^2\tilde{\tilde{\psi}}}{\partial z^2}. \tag{16}$$

The general solutions of equations (9) and (10) can be written as

- for $z\in[0,h-0]$,

$$\tilde{\tilde{\phi}}=A_1\exp(zR_L)+A_2\exp(-zR_L),\quad \tilde{\tilde{\psi}}=A_3\exp(zR_T)+A_4\exp(-zR_T); \tag{17}$$

- for $z \in [h+0, h+H]$,

$$\tilde{\tilde{\phi}} = A_5 \exp(zR_L) + A_6 \exp(-zR_L), \quad \tilde{\tilde{\psi}} = A_7 \exp(zR_T) + A_8 \exp(-zR_T); \tag{18}$$

where $R_L = \sqrt{k^2 - \omega^2/(c_L^2 - \mathrm{i}\omega(\lambda^* + 2\mu^*)/\rho)}$, $R_T = \sqrt{k^2 - \omega^2/(c_T^2 - \mathrm{i}\omega\mu^*/\rho)}$.

Substitution of equations (17) and (18) into equations (14)–(16) allows one to express the Fourier displacements $\tilde{\tilde{u}}$, $\tilde{\tilde{w}}$ and the Fourier stresses $\tilde{\tilde{\sigma}}_{zz}$, $\tilde{\tilde{\sigma}}_{xz}$ via the unknown constants $A_j$, $j = 1, \ldots, 8$. The relationships obtained by this substitution are given in Appendix A by equation (A1). Substituting equation (A1) into the equation of the beam motion (11), the interface conditions (12) and the boundary conditions (13), one obtains a linear system of eight algebraic equations with respect to $A_j$. This system may be written in the following form (a repeated subscript implies a summation):

$$a_{ij}A_j = \tilde{P}(\omega - kV)^* F_i, \tag{19}$$

where expressions for $a_{ij}$ and $F_i$ are given in Appendix A by equation (A2).

According to the Kramer's rule, the solution of system of algebraic equations (19) can be expressed as

$$A_j = \tilde{P}(\omega - kV)\Delta_j(k, \omega)/\Delta(k, \omega), \tag{20}$$

where $\Delta = \det([a_{ij}])$ is the determinant of the eigenmatrix $[a_{ij}]$ and $\Delta_j$ is the determinant of a modified matrix $[\tilde{a}_{ij}]$, where column $j$ of the eigenmatrix is replaced by the source vector $F$.

Analytic expressions for $\Delta$ and $\Delta_j$ have been calculated using Maple V Release 5 (Waterloo Maple Inc.).

As mentioned in the introduction, the main objective of this paper is the analysis of the layer surface vibration. To find expressions for the surface displacements one has to substitute equation (20) into the first and second equations of (A1) and let $n = 0$. This yields

$$\begin{aligned} \tilde{\tilde{u}}(k, 0, \omega) &= \tilde{P}(\omega - kV)\tilde{\tilde{u}}_0(k, \omega), \\ \tilde{\tilde{w}}(k, 0, \omega) &= \tilde{P}(\omega - kV)\tilde{\tilde{w}}_0(k, \omega), \end{aligned} \tag{21}$$

where

$$\tilde{\tilde{u}}_0(k, \omega) = \frac{1}{\Delta(k, \omega)} (\mathrm{i}k[\Delta_1(k, \omega) + \Delta_2(k, \omega)] + R_T(k, \omega)[\Delta_3(k, \omega) - \Delta_4(k, \omega)]),$$

$$\tilde{\tilde{w}}_0(k, \omega) = \frac{1}{\Delta(k, \omega)} (R_L(k, \omega)[\Delta_1(k, \omega) - \Delta_2(k, \omega)] - \mathrm{i}k[\Delta_3(k, \omega) + \Delta_4(k, \omega)]),$$

Applying the inverse Fourier transforms to equation (21), one obtains the following general expressions for the steady state response of the layer surface to the moving load $P(t)$:

$$\{u(x, 0, t), w(x, 0, t)\} = \frac{1}{4\pi^2} \int_{-\infty}^{+\infty} \int_{-\infty}^{+\infty} \tilde{P}(\omega - kV)\{\tilde{\tilde{u}}_0(k, \omega), \ \tilde{\tilde{w}}_0(k, \omega)\} \exp(-\mathrm{i}(\omega t - kx)) \, \mathrm{d}k \, \mathrm{d}\omega, \tag{22}$$

where the curly brackets here and further denote a vector consisting of two components.

In the following sections three types of variation of the load amplitude will be considered, namely the constant load $P(t) = P_0$, the harmonically varying load $P(t) = P_0 \cos(\Omega t)$ and a random stationary load $P(t)$. All three types of loading, after a substantially long time, lead to the steady state vibrations of the structure in the reference system moving with the load. In the steady state regime, all points of the layer surface experience exactly the same motion, with a certain time-shift. Therefore, to realize the steady state response to the surface it is sufficient to study vibrations of any point on the surface. We will use the point $x = 0$, where the displacements, according to equation (22), are given as

$$\{u(0,0,t), w(0,0,t)\} = \frac{1}{4\pi^2} \int_{-\infty}^{+\infty} \int_{-\infty}^{+\infty} \tilde{P}(\omega - kV) \{\tilde{\tilde{u}}_0(k,\omega),\ \tilde{\tilde{w}}_0(k,\omega)\} \exp(-\mathrm{i}\omega t \,\mathrm{d}k \,\mathrm{d}\omega. \quad (23)$$

Consequently, the amplitude spectra of vibrations in this point read

$$\{u_f(f), w_f(f)\} = \int_{-\infty}^{+\infty} \{u(0,0,t), w(0,0,t)\} \exp(-2\pi \mathrm{i} f t) \,\mathrm{d}t$$

$$= \frac{1}{2\pi} \int_{-\infty}^{+\infty} \tilde{P}(-2\pi f - kV) \{\tilde{\tilde{u}}_0(k, -2\pi f), \tilde{\tilde{w}}_0(k, -2\pi f)\} \,\mathrm{d}k, \quad (24)$$

where, to accomplish the integration over time, the following integral representation of the delta function has been used [9]:

$$\delta(\omega) = \frac{1}{2\pi} \int_{-\infty}^{+\infty} \exp(\mathrm{i}\omega t) \,\mathrm{d}t. \quad (25)$$

## 4. DISPERSION RELATION

Before starting the analysis of the system response to the different types of loading, it is worth discussing the dispersion relation for waves in the considered structure. This relation, having the form $f = K(k)$, $\{f, k\} \in \Re$, couples the wave number $k$ and the frequency $f = \omega/2\pi$ of waves, which can propagate along the $x$-axis without attenuation. Mathematically, the relation $f = F(k)$ is the real solution of the equation

$$\lim_{\{\lambda^*, \mu^*\} = 0} \Delta(k, 2\pi f) = 0. \quad (26)$$

In Figure 2 the dispersion relation is plotted as a solid line for the following set of the system parameters:

$$\begin{aligned} &E_{layer} = 3 \times 10^7 \text{ N/m}^2, \quad \nu = 0{\cdot}3, \quad \rho = 1700 \text{ kg/m}^3, \quad h = 12 \text{ m}, \quad H = 15 \text{ m}, \\ &\rho_B/a = 3 \times 10^4 \text{ kg/m}^2, \quad EI/a = 10^9 \text{ N m}, \end{aligned} \quad (27)$$

representing a realistic, though arbitrary soft ground, and some characteristics of the train tunnel.

Along with the dispersion curve, Figure 2 contains three straight lines starting at the origin and a set of dashed curves. The straight lines show the phase velocities $V_{ph} = \omega/k = 2\pi f/k$ equal to the Rayleigh wave velocity $c_R$, the shear wave velocity $c_T$ and the compression wave velocity $c_L$ in the layer. The dashed curves represent waves, which may propagate in the $x$ direction with a slight attenuation and may be mathematically found as minima of the function $|\Delta(k, 2\pi f)|$ for real $k$ and $f$. It will be shown that these slightly attenuated waves play an important role in the dynamic structural response.

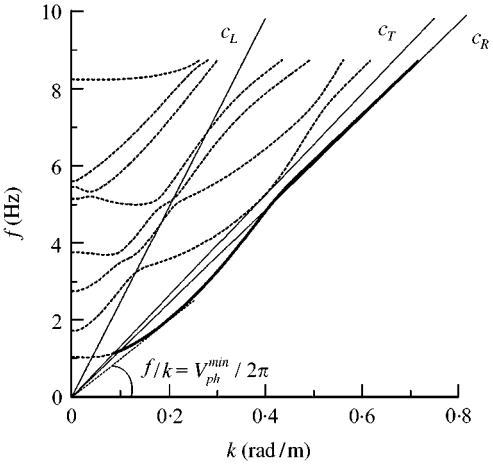


Figure 2. Dispersion curves.

One can see from Figure 2 that the bold curve lies below the straight line $V_{ph} = c_T$, which means that the phase velocity of any wave propagating with a constant amplitude is smaller than the velocity of the shear wave in the layer. This implies that the bulk waves in the layer are not involved in this wave motion. Therefore, the propagating waves are either the "beam waves" localized near the beam or the surface waves localized near the layer surface. The dispersion curve (the bold line) clearly shows that the long waves (small $k$) appear to be the "beam waves" and the shorter waves are the Rayleigh surface waves.

The slightly attenuated waves, whose dispersion curves are depicted by the dashed lines, have phase velocities larger than the shear wave velocity $c_T$. Thus, these waves represent the wave motion of the layer. The reason for them to be attenuated is the beam, which, being much stiffer than the layer material, quickly transfers the energy of the layer motion into the energy of its own vibration. One can say that the beam serves as an equivalent damper for the wave motion of the layer. This equivalent damping, however, can be not so extreme and, therefore, the slightly attenuated wave motion of the layer can play an important role in the structural response.

One of the most important issues for the following analysis, reflected by Figure 2, is that the minimal phase velocity $V_{ph}^{min}$ of waves propagating in the structure is noticeably smaller than the Rayleigh wave velocity $c_R$ (one can calculate that $V_{ph}^{min} = 68$ m/s and $c_R = 77$ m/s). This result is important since $V_{ph}^{min}$ is the critical velocity of the constant load, moving along the beam. It is critical in the following two senses. First, if the load moves with the velocity $V = V_{ph}^{min}$, the amplification of the steady state response takes place [10–12]. Secondly, the relation between the load velocity $V$ and $V_{ph}^{min}$ determines whether or not waves are excited in the structure. If $V < V_{ph}^{min}$, the field generated by the load in the stationary regime is localized around the loading point and there are no waves propagating away from the load. On the contrary, if the load velocity exceeds $V_{ph}^{min}$, the load radiates waves, providing an oscillatory response of the structure at quite distanced points.

Thus, the minimal phase velocity $V_{ph}^{min}$ is the basic parameter to be known for analysis of the structural response to the moving load. It is of interest to know how $V_{ph}^{min}$ is effected by the depth of the tunnel. To show this, the dependence of $V_{ph}^{min}$ upon the distance $h$ between the layer surface and the beam ($H$ is kept constant) is plotted in Figure 3.

One can see from the figure that the larger the distance $h$, the larger the minimal phase velocity. This implies that the deeper the tunnel, the larger the critical velocity of a train

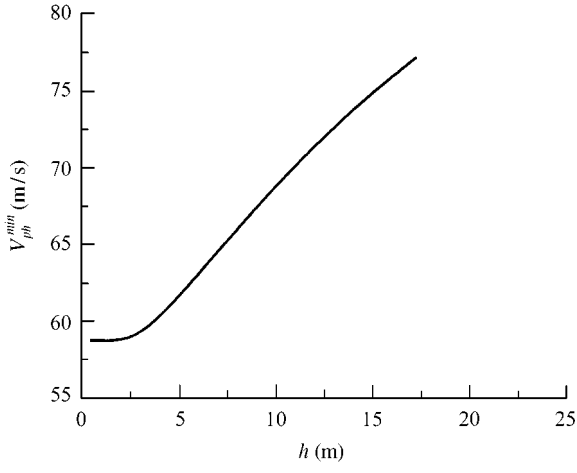


Figure 3. Minimal phase velocity versus distance between the beam and the layer surface.

moving in this tunnels. Therefore, to increase the critical velocity of a high-speed train it is favourable to let the train move in a deep tunnel.

## 5. RESPONSE TO THE CONSTANT LOAD

The vertical force, a moving train acts upon the rail with, is a rather complicated function of time. The spectrum of this function is starting from zero frequency and lasts up to hundreds of Hz. This spectrum reflects the train vibration as a rigid body, the vibration due to non-roundness of the wheels, the sleeper passing frequency, etc. However, a significant part of the loading energy is concentrated around the zero frequency. This is due to the gravity force, providing constant pressure on the rails. To analyze the structural response to this pressure, in this section the motion of the constant load $P(t) = P_0$ is considered. In this case, by employing the representation (25), one may obtain the following expression for $\tilde{P}(\omega - kV)$:

$$\tilde{P}(\omega - kV) = \int_{-\infty}^{+\infty} P_0 \exp(\mathrm{i}t(\omega - kV))\,\mathrm{d}t = 2\pi P_0\,\delta(\omega - kV). \tag{28}$$

Consequently, expressions (23) and (24) for the displacements and the spectra at the point $\{x = 0,\ z = 0\}$ take the form

$$\{u(0,0,t),\ w(0,0,t)\} = \frac{P_0}{2\pi}\int_{-\infty}^{+\infty} \{\tilde{\tilde{u}}_0(k,kV),\ \tilde{\tilde{w}}_0(k,kV)\}\ \exp(-\mathrm{i}kVt)\,\mathrm{d}k, \tag{29}$$

$$\{u_f(f),\ w_f(f)\} = \frac{P_0}{V}\left\{\tilde{\tilde{u}}_0\left(-\frac{2\pi f}{V}, -2\pi f\right),\ \tilde{\tilde{w}}_0\left(-\frac{2\pi f}{V}, -2\pi f\right)\right\}. \tag{30}$$

As one can see, the displacements in this case are expressed in the form of the single Fourier integral, which can be easily treated numerically, and the spectra are found as algebraic expressions.

In Figure 3 the modulus of the amplitude spectra is shown calculated by the formula $|u_f| = \sqrt{(\mathrm{Re}(u_f))^2 + (\mathrm{Im}(u_f))^2}$, $|w_f| = \sqrt{(\mathrm{Re}(w_f))^2 + (\mathrm{Im}(w_f))^2}$. The set of parameters (27) has been used for calculations and, additionally,

$$P_0/a = 10^4 \text{ N/m}, \quad \lambda^* = \mu^* = 3 \times 10^4 \text{ kg/ms}. \tag{31}$$

The load magnitude $P_0$ in equation (32) is chosen to describe the axle loading given by a train. Figure 4(a) is plotted for the sub-critical velocity $V = 30$ m/s, while Figure 4(b) shows the spectra in the super-critical motion $V = 75$ m/s (remember that according to Figure 3, the critical velocity in the considered case in about $V_{cr} = V_{ph}^{min} = 68$ m/s). The curve starting from the origin is related to the spectrum of the horizontal displacement $u_f$ and the other curve to the spectrum of $w_f$.

One can see from Figure 4 that in both the sub-critical and the super-critical cases, a significant part of the spectrum is located in the lower frequency band. However, in the super-critical case, the spectrum is approximately twice as wide and has a noticeable part located above 4 Hz. The other specific feature of the super-critical case is that the spectrum has two maxima (if there was no viscosity in the layer, these maxima would become infinite). These maxima arise due to the radiation of waves by the moving load. The frequencies of the waves can be easily found graphically in the manner shown in Figure 5. This figure includes the dispersion curves of the structure and the straight line $\omega = kV \Leftrightarrow f = kV/2\pi$, which is called the "kinematic invariant" [3, 13]. Mathematically, the relation $\omega = kV$ provides the non-triviality of the Delta function in equation (28). Physically, this relation implies that the phase velocity $V_{ph} = \omega/k$ of all waves radiated by the constant load must be equal to the velocity $V$ of the load, see references [12, 13]. The crossing points of the kinematic invariant and the dispersion curves give the following frequencies of the radiated waves:

$$f_1 \approx 1{\cdot}23 \text{ Hz}, \quad f_2 \approx 4{\cdot}68 \text{ Hz}. \tag{32}$$

These frequencies are obviously in agreement with Figure 4(b).

One can see from Figure 5 that for the load velocities higher than the shear wave velocity $c_T$, the kinematic invariant may not have crossing points with the dispersion branch describing the non-attenuating waves (the solid bold curve). However, there is always a number of crossing points with the dashed lines, which represent the slightly attenuated

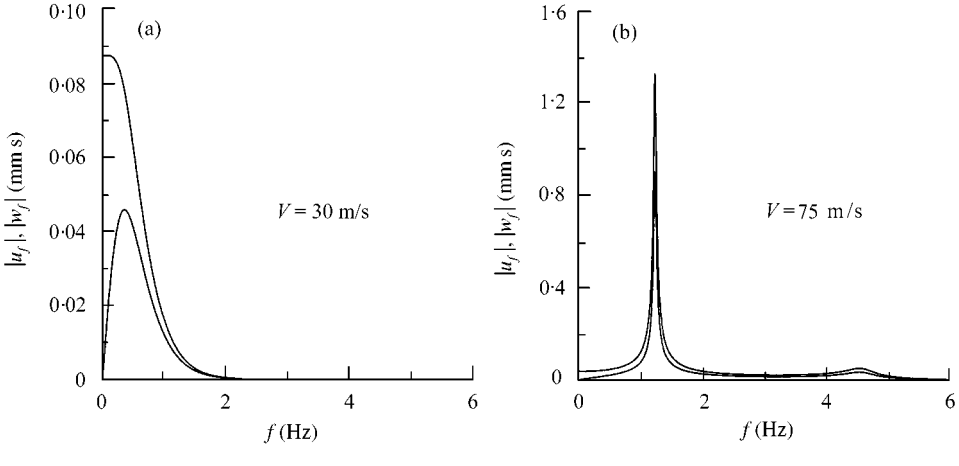


Figure 4. The amplitude spectra.

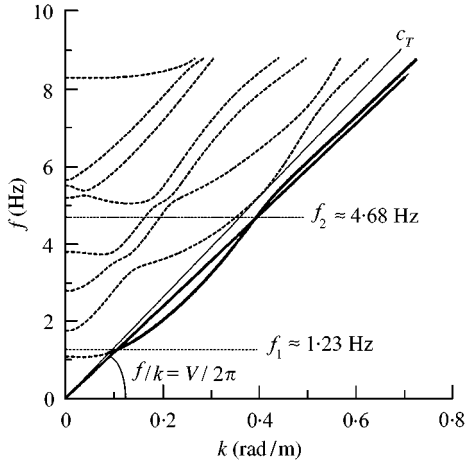


Figure 5. Graphical determination of the frequencies of waves radiated at $V = 75$ m/s

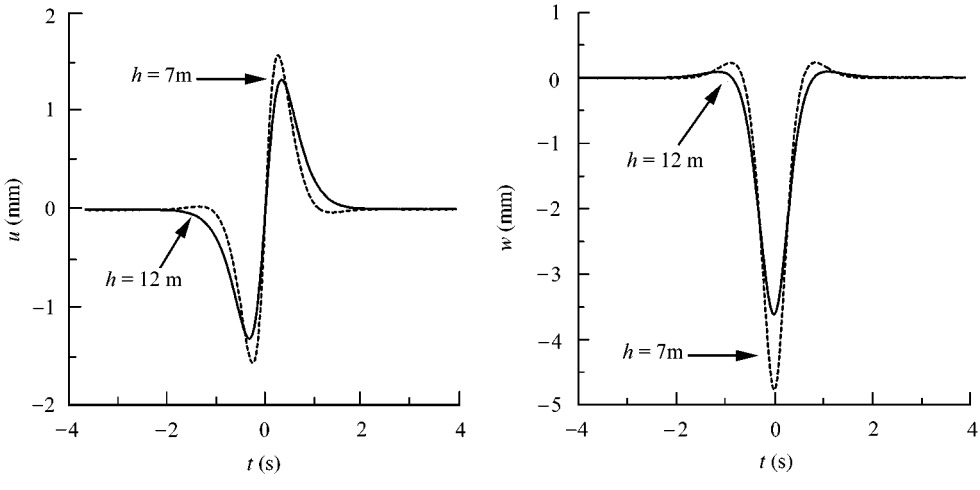


Figure 6. The surface displacement for $V = 30$ m/s.

waves in the structure. As analysis shows, these crossing points provide certain amplification in the response spectra.

Let us analyze the displacements $u(0, 0, t)$ and $w(0, 0, t)$ of the layer surface. To this end one has to evaluate the single integral in equation (29). It can be simply done numerically, since the integral kernel has no singularities and quickly vanishes as $|k| \to \infty$. Results of the numerical evaluation of equation (29) are presented in Figures 6 and 7, where the displacements versus time are plotted. Figure 6 reflects the sub-critical case $V = 30$ m/s and Figure 7 is related to the super-critical load moving with $V = 75$ m/s. Every figure shows two lines: the solid line is plotted for $h = 12$ m and the dashed line for $h = 7$ m. The other parameters of the system are fixed by the sets (27) and (31).

Analysing the figures, the following conclusions can be drawn:

1. In the sub-critical case depicted in Figure 6, the observation point ($x = 0$, $z = 0$) experiences a short, about 4 s, impulse-like deflection. The impulse is almost perfectly

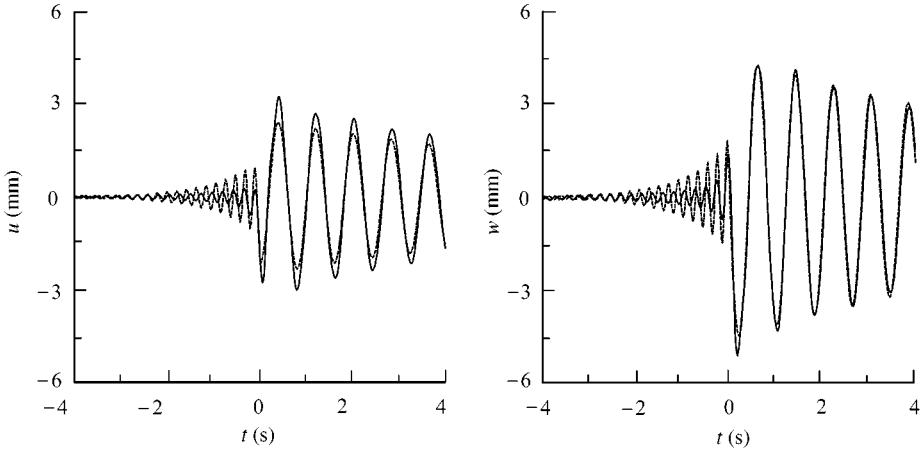


Figure 7. The surface displacements for $V = 75$ m/s.

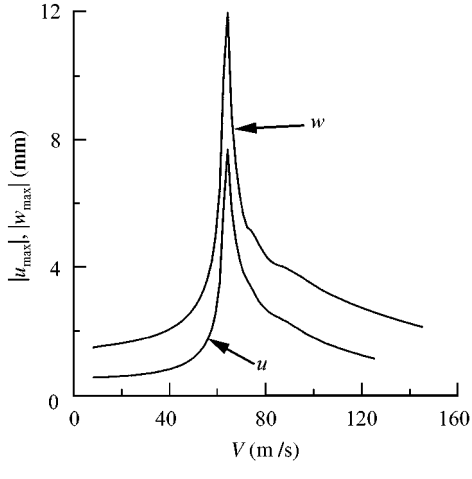


Figure 8. The maximum displacements versus load velocity.

symmetric vertically and antisymmetric horizontally with respect to the time instant $t = 0$ when the load passes the observation point. Concerning the effect of the distance $h$ between the beam and the layer surface, one can see that the length of the impulse is almost not affected by $h$, while the impulse amplitude is affected slightly.

2. In the super-critical case depicted in Figure 7, the observation point vibrates much longer and the vibration pattern becomes wave-like. This happens due to the fact that the load radiates waves into the layer. One can see from Figure 7 that the wave pattern for $t < 0$ has a higher frequency and smaller amplitude than that for $t > 0$. The difference in frequencies is because of the Doppler effect, implying that an observed wave possesses a higher frequency when the load moves towards the observation point ($t < 0$) and, on the other hand, the wave frequency becomes smaller when the distance between the load and the observation point grows ($t > 0$). The difference in the amplitudes directly follows from the difference in the frequencies. This is since the Voigt solid is used to model the layer.

To show the effect of the load velocity on the surface response, in Figure 8 the modulus of the maximum displacements of the observation point versus the velocity is plotted.

Figure 8 shows that the maximum displacement of the observation point depends on the load velocity in the resonance manner. The highest amplification takes place when the load velocity is equal to the minimal phase velocity of waves in the structure. This velocity, according to Figures 2 and 3 is about 68 m/s for the chosen $h = 12$ m.

## 6. RESPONSE TO A HARMONICALLY VARYING LOAD

As mentioned in the beginning of the previous section, the loading spectrum produced by a moving train is rather wide. To study the effect of the train vibrations on the structural response, a harmonic variation of the load magnitude is considered in this section. The load reads $P(t) = P_0 \cos(\Omega t)$ and by employing the integral representation of the delta function, equation (25) may be transformed as

$$\tilde{P}(\omega - kV) = \int_{-\infty}^{+\infty} P_0 \cos(\Omega t) \exp(\mathrm{i}t(\omega - kV))\,\mathrm{d}t = \pi P_0 (\delta(\omega - kV + \Omega) + \delta(\omega - kV - \Omega)). \tag{33}$$

Substituting expression (33) into equation (23) and equation (24), one obtains

$$\{u(0,0,t),\ w(0,0,t)\} = \frac{P_0}{4\pi} \int_{-\infty}^{+\infty} [\{\tilde{\tilde{u}}_0(k, kV - \Omega),\ \tilde{\tilde{w}}_0(k, kV - \Omega)\} \exp(-\mathrm{i}(kV - \Omega)t) + \{\tilde{\tilde{u}}_0(k, kV + \Omega),\ \tilde{\tilde{w}}_0(k, kV + \Omega)\} \exp(-\mathrm{i}(kV + \Omega)t)]\,\mathrm{d}k \tag{34}$$

$$\{u_f(f),\ w_f(f)\} = \frac{P_0}{2V} \left[ \left\{ \tilde{\tilde{u}}_0 \left( \frac{\Omega - 2\pi f}{V}, -2\pi f \right),\ \tilde{\tilde{w}}_0 \left( \frac{\Omega - 2\pi f}{V}, -2\pi f \right) \right\} + \left\{ \tilde{\tilde{u}}_0 \left( \frac{-2\pi f - \Omega}{V}, -2\pi f \right),\ \tilde{\tilde{w}}_0 \left( \frac{-2\pi f - \Omega}{V}, -2\pi f \right) \right\} \right]. \tag{35}$$

Within the scope of this paper, the most pronounced difference between the structural response to constant and to the harmonic load is that the latter may radiate waves by moving with much smaller velocities or even being fixed at a point. This is due to the following relationship, the angular frequency $\omega$ of radiated wave and the load frequency $\Omega$ must satisfy:

$$\omega = kV \pm \Omega. \tag{36}$$

This relationship follows, for example, from equation (33) by letting the arguments of the delta functions be equal zero. The kinematic invariant, determined by equation (36) is shown in Figure 9 for $V = 30$ m/s and $f_\Omega = \Omega/2\pi = 2$ Hz by the bold straight line (the plus sign in equation (36) is used). The chosen frequency is approximately equal to the eigenfrequency of the vertical wagon vibration. In the same figure, the dispersion curves of the structure are plotted by employing the parameter sets (27) and (31). The dispersion curves are plotted both for positive and negative wave numbers. This is necessary since, in contrast to the constant load, the harmonically varying load can radiate waves with a negative phase velocity.

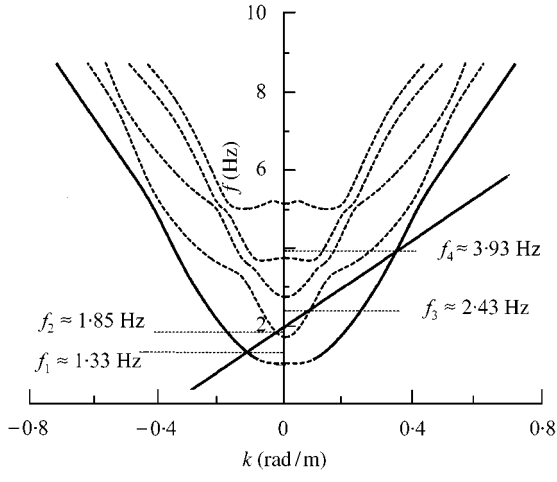


Figure 9. Graphical determination of the frequencies of waves radiated by the harmonic load ($f_\Omega = 2$ Hz, $V = 30$ m/s).

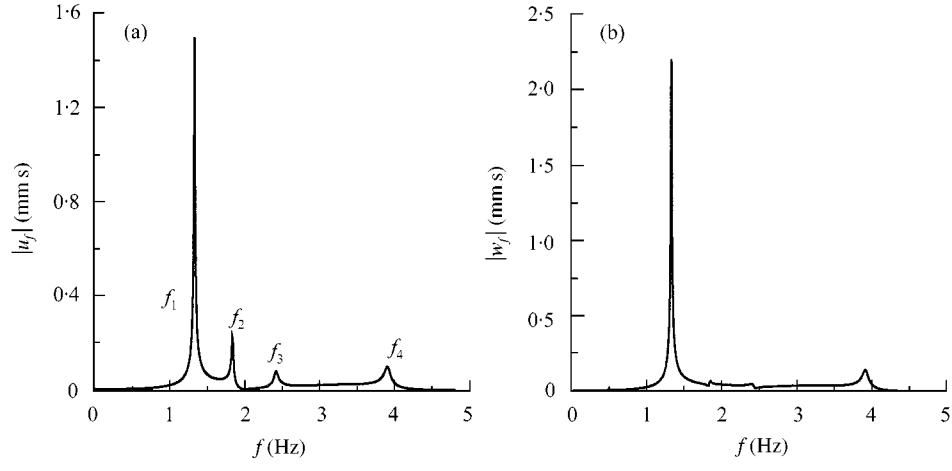


Figure 10. Amplitude spectra of the surface displacements for $f_\Omega = 2$ Hz, $V = 30$ m/s.

Figure 9 obviously shows that the harmonic load, moving with the velocity $V = 30$ m/s (about 45% of the minimal phase velocity $V_{ph}^{min}$) radiates four waves. Two of these waves are the interface waves ($f_1$ and $f_4$) and the other two are the body waves. Information about the amplitudes of the radiated waves can be obtained by analyzing the spectra of the surface vibrations depicted in Figure 10.

One can see from Figure 10 that both the interface waves and the body waves give some amplification in the response spectrum. Since we take into account the viscosity in the layer, all maxima of the spectra are limited. The resonance peaks related to the interface waves are limited by the viscosity in the layer and would become infinite in its absence. The peaks caused by the body waves are bounded due to the viscosity and the energy extraction along the beam. Therefore, if the purely elastic layer would be considered, these peaks remained finite. Figure 10 shows that the largest amplification takes place at the lowest frequency $f_1$

of the interface waves. The other frequencies behave differently in the spectrum $u_f$ of the horizontal vibration and in the spectrum $w_f$ of the vertical vibration. In the vertical direction the body waves ($f_2$ and $f_3$) provide almost no amplification, while in the horizontal direction the response of the frequencies $f_2$, $f_3$ and $f_4$ is approximately the same. This difference is dictated by the boundary conditions (3) at the beam interface. According to these conditions, the beam vibrates only vertically and, consequently, it extracts much less energy from the horizontal layer vibration than from the vertical one. Therefore, the extraction of energy by the beam vibrations (the equivalent radiation damping) is very small in the horizontal direction and the resonance peaks caused by the body waves are significantly only in the spectrum $u_f$.

By increasing the load frequency the spectrum of the surface vibrations becomes wider and more complicated, but the resonance peaks are less pronounced. One can see this from Figure 11, where the spectra $|u_f|$ and $|w_f|$ are depicted for the same load velocity $V = 30$ m/s, but for double the higher frequency $f_\Omega = 4$ Hz.

The expansion of the spectrum towards the frequency is simply understood from Figure 9. Indeed, to find the frequencies of waves radiated by the load for the frequency $f_\Omega = 4$ Hz, the kinematic invariant (the bold straight line) is translated towards the higher frequencies in order to cross the frequency axis at the point $f = 4$ Hz. Obviously, in this case there will be more crossing points of the kinematic invariant and the dispersion curves. These new crossing points will appear at higher frequencies, providing the widening of the spectrum. The limitation of the resonance peaks is directly related to the shifting of the spectrum towards the higher frequencies, which are harder damped.

The surface displacements $u(0, 0, t)$ and $w(0, 0, t)$ for $f_\Omega = 2$ Hz, $V = 30$ m/s are depicted in Figure 12, showing that the observation point on the surface experiences a vibratory motion, which lasts quite a long time.

The pattern of the horizontal vibration is more complicated than that of the vertical vibration. This is in perfect agreement with Figure 10, which shows that the spectrum of the horizontal vibration contains four resonance frequencies, while the spectrum of the vertical vibration possesses only two. One can see from Figure 12 that the vibrations at $t < 0$ have higher frequencies and smaller amplitudes than at $t > 0$. This is because of the Doppler effect as discussed in the previous section for the case of super-critically moving constant load.

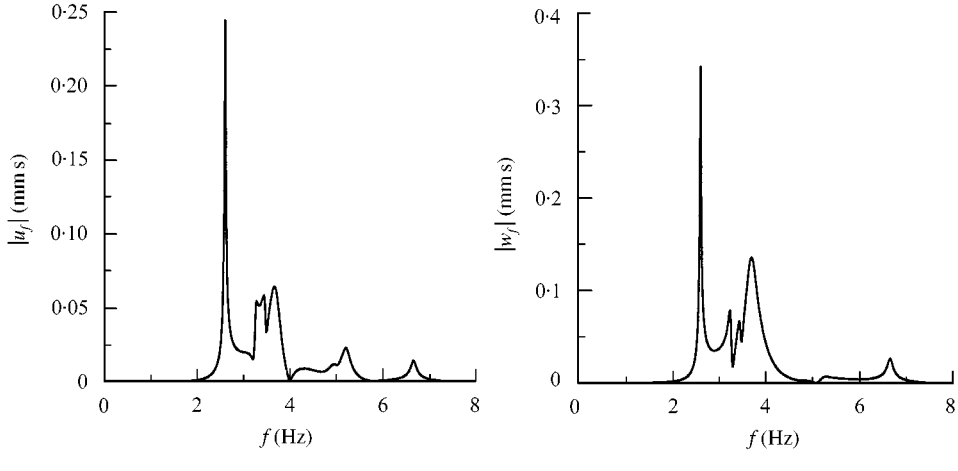


Figure 11. Amplitude spectra of the surface displacements for $f_\Omega = 4$ Hz, $V = 30$ m/s.

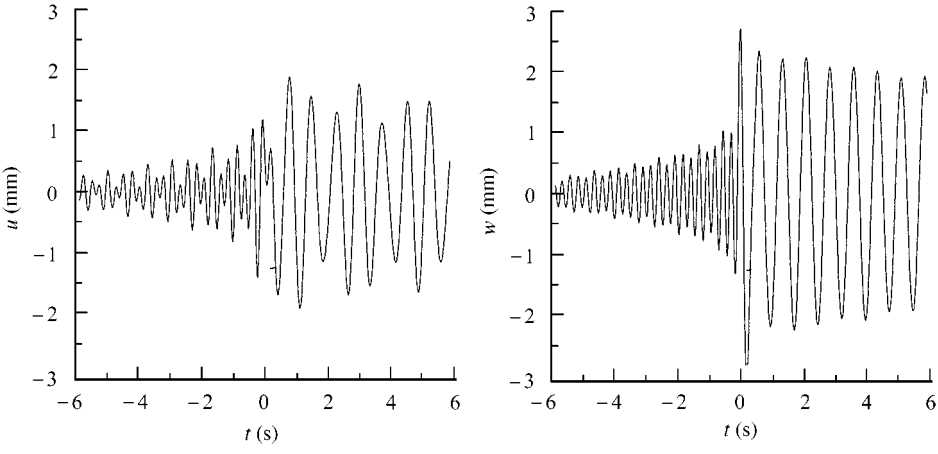


Figure 12. The surface displacements for $f_\Omega = 2$ Hz, $V = 30$ m/s.

Analysis shows that at higher load frequencies the displacement pattern becomes more complicated since the spectrum of vibrations contains more resonance frequencies, see Figure 11. The amplitude of the vibrations becomes smaller due to the spectrum shifting towards the higher frequencies.

## 7. RESPONSE TO A RANDOM STATIONARY LOAD

In general, the loading force acting on rails is a complicated function of time. Wide variety of such functions may be considered by assuming a random character to the load. This assumption allows to take into account the wideness of the loading spectrum and to consider variation of the loading from train to train and from track to track. In this section, we suppose that the load is given by a stationary random function of time with zero mathematical expectation. For the following analysis this function is represented in the form

$$P(t) = \sum_{n=1}^{N} F_n(\Omega_n) \exp(\mathrm{i}(\Omega_n t + \varphi_n)), \tag{37}$$

where $\Omega_n$ and $F(\Omega_n)$ are deterministic parameters and $\varphi_n$ is a random variable uniformly distributing over the range $[0, 2\pi]$.

Substituting equation (37) into the expression for $\tilde{P}(\omega)$, one obtains

$$\begin{aligned}\tilde{P}(\omega - kV) &= \int_{-\infty}^{+\infty} P(t) \exp(\mathrm{i}t(\omega - kV))\,\mathrm{d}t \\ &= \int_{-\infty}^{+\infty} \sum_{n=1}^{N} F_n(\Omega_n) \exp(\mathrm{i}(\Omega_n t + \varphi_n)) \exp(\mathrm{i}t(\omega - kV))\,\mathrm{d}t \\ &= 2\pi \sum_{n=1}^{N} F_n(\Omega_n) \exp(\mathrm{i}\varphi_n)\, \delta(\omega - kV + \Omega_n). \end{aligned} \tag{38}$$

Accordingly, equation (23) describing the displacements $[u(0,0,t),\ w(0,\ 0,\ t)\}$, which are now random functions of time, is

$$\{u(0,\ 0,\ t),\ w(0,\ 0,\ t)\}$$

$$= \frac{1}{2\pi}\int_{-\infty}^{+\infty}\int_{-\infty}^{+\infty}\sum_{n=1}^{N} F_n(\Omega_n)\exp(\mathrm{i}\varphi_n)\delta(\omega - kV + \Omega_n)\{\tilde{\tilde{u}}_0(k,\omega),\ \tilde{\tilde{w}}_0(k,\omega)\}\exp(-\mathrm{i}\omega t)\,\mathrm{d}k\mathrm{d}\omega$$

$$= \frac{1}{2\pi}\int_{-\infty}^{+\infty}\sum_{n=1}^{N} F_n(\Omega_n)\exp(\mathrm{i}\varphi_n)\{\tilde{\tilde{u}}_0(k,kV-\Omega_n),\ \tilde{\tilde{w}}_0(k,kV-\Omega_n)\}\exp(-\mathrm{i}(kV-\Omega_n)t)\mathrm{d}k \tag{39}$$

Evidently, for the considered load with zero mathematical expectation $\langle P(t)\rangle = 0$, the mathematical expectations of $u(0,0,t)$ and $w(0,0,t)$ are trivial. Therefore, the auto-covariance functions of the response are analyzed in this paper. According to reference [14], these functions are defined as

$$R_{uu}(t,\ t+\tau) = \int_{\varphi} u(0,\ 0,\ t)\,u^*(0,\ 0,\ t+\tau)\ f(\boldsymbol{\varphi})\ \mathrm{d}\boldsymbol{\varphi},$$

$$R_{ww}(t,\ t+\tau) = \int_{\varphi} w(0,\ 0,\ t)\,w^*(0,\ 0,\ t+\tau)\ f(\boldsymbol{\varphi})\ \mathrm{d}\boldsymbol{\varphi}, \tag{40}$$

where $\boldsymbol{\varphi}$ is a vector with components $\varphi_k$, $f(\boldsymbol{\varphi}) = 1/(2\pi)^N$ is the probability density, the integration over each $\varphi_k$ takes place from zero to $2\pi$ and the asterisk denotes the complex conjugation.

By substituting equation (39) into equation (40) one may obtain the following expression for $R_{uu}(t,\ t+\tau)$ (expression for $R_{ww}(t,t+\tau)$ may be obtained analogously):

$$R_{uu}(t,\ t+\tau) = \frac{1}{4\pi^2}\int_{-\infty}^{+\infty}\int_{-\infty}^{+\infty}\sum_{n=1}^{N} F_n(\Omega_n)F_n^*(\Omega_n)\tilde{\tilde{u}}_0(k,kV-\Omega_n)\exp(-\mathrm{i}Vt(k-k_1))$$
$$\times\,\tilde{\tilde{u}}_0^*(k_1,\ k_1V-\Omega_n)\exp(\mathrm{i}(k_1V-\Omega_n)\tau)\,\mathrm{d}k\mathrm{d}k_1. \tag{41}$$

Details of obtaining equation (41) are given in Appendix B. Equation (41) shows that in contrast to the stationary loading process $P(t)$, the response $u(0,0,t)$ is non-stationary (the covariance function depends both on time and on the time shift $\tau$). This is due to the load motion with respect to the observation point.

In this paper, the attention is focused on the study of the variance of the displacements $u(0,0,t)$ and $w(0,0\,t)$. According to equation (41), the variance $\sigma_{uu}^2(t)$ of $u(0,0,t)$ reads

$$\sigma_{uu}^2(t) = R_{uu}(t,\ t) = \frac{1}{4\pi^2}\int_{-\infty}^{+\infty}\int_{-\infty}^{+\infty}\sum_{n=1}^{N} F_n(\Omega_n)F_n^*(\Omega_n)\tilde{\tilde{u}}_0(k,kV-\Omega_n)\exp(-\mathrm{i}Vt(k-k_1))$$
$$\times\,\tilde{\tilde{u}}_0^*(k_1,\ k_1V-\Omega_n)\ \mathrm{d}k\mathrm{d}k_1$$
$$= \frac{1}{4\pi^2}\sum_{n=1}^{N}|F_n(\Omega_n)|^2\left|\int_{-\infty}^{+\infty}\tilde{\tilde{u}}_0(k,kV-\Omega_n)\exp(-\mathrm{i}kVt)\ \mathrm{d}k\right|^2, \tag{42}$$

where the vertical lines $|\cdots|$ denote the modulus of a complex function. Further reduction of equation (42) can be fulfilled by introducing the spectral density $S_{PP}(\Omega)$ of the load $P(t)$

given as

$$\lim_{\Delta\omega \to 0} S_{PP}(\Omega_n)\,\Delta\omega = |F_n(\Omega_n)|^2, \quad (\Delta\omega = \omega_{n+1} - \omega_n). \tag{43}$$

Substitution of representation (43) into equation (42) yields the following expression for the variance $\sigma^2_{uu}(t)$:

$$\sigma^2_{uu}(t) = \frac{1}{4\pi^2} \int_{-\infty}^{+\infty} S_{PP}(\Omega) \left| \int_{-\infty}^{+\infty} \tilde{\tilde{u}}_0(k, kV - \Omega) \exp(-\mathrm{i}kVt)\, \mathrm{d}k \right|^2 \mathrm{d}\Omega. \tag{44}$$

The variance of the function $w(0,0,t)$ can be obtained in the exactly same manner to give

$$\sigma^2_{ww}(t) = R_{ww}(t,\, t) = \frac{1}{4\pi^2} \int_{-\infty}^{+\infty} S_{PP}(\Omega) \left| \int_{-\infty}^{+\infty} \tilde{\tilde{w}}_0(k, kV - \Omega) \exp(-\mathrm{i}Vkt)\, \mathrm{d}k \right|^2 \mathrm{d}\Omega. \tag{45}$$

It is important to underline that the integrands in expressions (44) and (45) have nothing to do with the instantaneous spectral densities $S_{uu,ww}(\omega, t)$ defined by the Wiener–Khinchin relations

$$R_{uu,ww}(t, t+\tau) = \int_{-\infty}^{+\infty} S_{uu,ww}(\omega,\, t) \exp(\mathrm{i}\omega\tau)\, \mathrm{d}\omega,$$

$$S_{uu,ww}(\omega,\, t) = \frac{1}{2\pi} \int_{-\infty}^{+\infty} R_{uu,ww}(t,\, t+\tau) \exp(-\mathrm{i}\omega\tau)\, \mathrm{d}\tau.$$

As follows from these relations, the variance of the displacements $u(0,0,t)$ and $w(0,0,t)$ reads

$$\sigma^2_{uu,ww}(t) = R_{uu,ww}(t,\, t) = \int_{-\infty}^{+\infty} S_{uu,ww}(\omega,\, t)\, \mathrm{d}\omega$$

and one could intend to relate the integrands in equations (44) and (45) to $S_{uu,ww}(\omega, t)$. This would be, however, a wrong intention since correct expressions for $S_{uu,ww}(\omega, t)$ are given as

$$S_{uu}(\omega,t) = \frac{1}{4\pi^2} \int_{-\infty}^{+\infty} \int_{-\infty}^{+\infty} S_{PP}(k_1 V - \omega)\tilde{\tilde{u}}_0(k, kV - k_1 V + \omega)\tilde{\tilde{u}}_0^*(k_1, \omega)\exp(\mathrm{i}Vt(k_1 - k))\mathrm{d}k\mathrm{d}k_1$$

$$S_{ww}(\omega,t) = \frac{1}{4\pi^2} \int_{-\infty}^{+\infty} \int_{-\infty}^{+\infty} S_{PP}(k_1 V - \omega)\tilde{\tilde{w}}_0(k, kV - k_1 V + \omega)\tilde{\tilde{w}}_0^*(k_1, \omega)\exp(\mathrm{i}Vt(k_1 - k))\mathrm{d}k\mathrm{d}k_1$$

These expressions may be simply obtained by applying the Fourier transform over the time shift $\tau$ to equation (41) and using equation (43).

Although expressions

$$Z_u(\Omega, t) = \frac{1}{4\pi^2} \left| \int_{-\infty}^{+\infty} \tilde{\tilde{u}}_0(k, kV - \Omega)\exp(-\mathrm{i}Vkt)\mathrm{d}k \right|^2,$$

$$Z_w(\Omega, t) = \frac{1}{4\pi^2} \left| \int_{-\infty}^{+\infty} \tilde{\tilde{w}}_0(k, kV - \Omega)\exp(-\mathrm{i}Vkt)\mathrm{d}k \right|^2 \tag{46}$$

in equations (44) and (45) have no clear physical significance, their behavior is worth discussing. Indeed, these expressions contain information about the layer and do not

depend on the random properties of the load. In this sense, expressions (46) are of the same issue as the transfer function [14] of a linear deterministic system, which, undoubtedly, should be separately studied.

To draw conclusions concerning time, frequency and velocity dependence of the functions $Z_u(\Omega, t)$ and $Z_w(\Omega, t)$ it is sufficient to plot one. It is done in Figure 13 where the function $\tilde{Z}_w(\Omega, t) = \mu^2 Z_w(\Omega, t)$ is depicted versus the frequency $f = \Omega/(2\pi)$ for three different time moments: $t = -1$ s (dashed line), $t = 0$ (solid line), $t = +1$ s (dash-dotted line). Figure 13(a) shows the dependence for the sub-critical velocity $V = 30$ m/s and Figure 13(b) is related to the super-critical velocity $V = 75$ m/s.

Analyzing Figure 13 one can conclude the following:

1. The non-stationarity of the process $w(0, 0, t)$, which is determined by variation of $Z_w(\Omega, t)$ in time, is visible for both velocities. However, for the super-critical velocity $V = 75$ m/s this variation is more significant.
2. Function $Z_w(\Omega, t)$ has the largest local maximum at $f = 0{\cdot}74$ Hz for $V = 30$ m/s and at $f = 0{\cdot}35$ Hz for $V = 75$ m/s. This maximum can be understood with the help of Figure 14, which is an analogue to Figure 9. In Figure 14, the dispersion curves are plotted together with two straight lines (kinematic invariants). Line (1) is related to $f = 0{\cdot}74$ Hz; $V = 30$ m/s and line (2) to $f = 0{\cdot}35$ Hz; $V = 75$ m/s. Figure 14 obviously shows that both straight lines are tangential to one of the dispersion curves at the points marked by circles. This implies that the corresponding harmonic load excites in the structure a wave with the group velocity close to the velocity of the load and, therefore, the wave energy remains in the vicinity of the loading point and grows in time. As shown in references [3, 12, 13] this situation leads to the wave resonance in the structure and, accordingly, to the maximum in the dependence $Z_w(\Omega)$.
   Concerning the largest maximum, one can further notice that the magnitude of $Z_w(\Omega, t)$ in the maximum is significantly larger for in the sub-critical motion than in the super-critical. Once again this can be understood by using Figure 14, which shows that the straight line related to $V = 30$ m/s is tangential to the dispersion branch of the waves propagating with a constant amplitude and the line $V = 75$ m/s touches a branch of slightly attenuated waves. Evidently, in the first case the wave resonance is more pronounced and, consequently, the peak of $Z_w(\Omega)$ is larger.

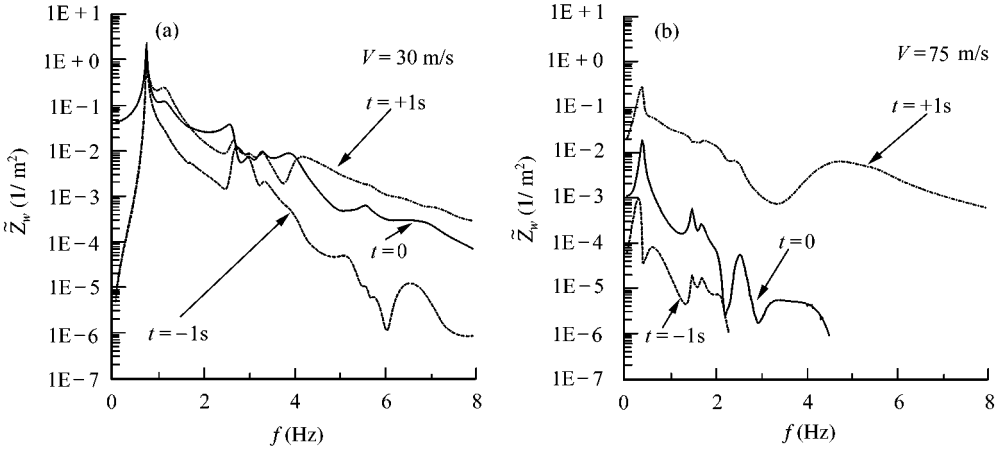


Figure 13. Function $\mu^2 Z_w(\Omega, t)$ versus frequency $f$ in the logarithmic (base 10) scale.

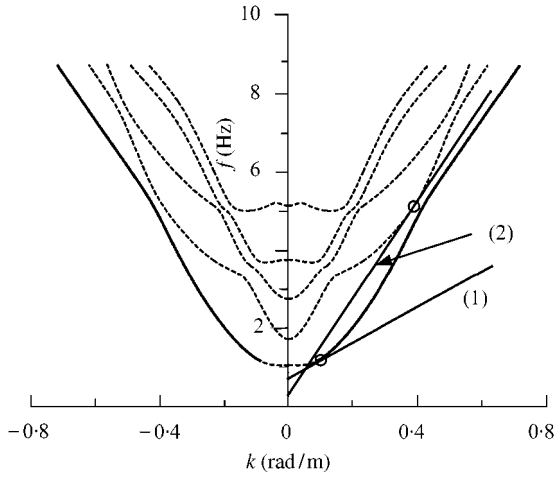


Figure 14. Dispersion curves and kinematic invariant lines. Line (1) — $f = 0{\cdot}74$ Hz and $V = 30$ m/s: Line (2) — $f = 0{\cdot}35$ Hz and $V = 75$ m/s.

3. Function $Z_w(\Omega, t)$ is non-monotonic with respect to the frequency. However, the general tendency (for $f > 1$ Hz) is that the function decreases with frequency. This decrease is quite steep, which implies that high frequencies in the loading spectrum make a minor contribution into the variance of the function $w(0, 0, t)$.

Let us finally discuss the variances $\sigma^2_{uu,ww}(t)$. To find them numerically one has to know the spectral density of the load $S_{PP}(\Omega)$. In practice, this function is quite complicated, but in the lower frequency band (below 10 Hz) it may be described by the spectral density of the white noise given as [14].

$$S_{PP}(\Omega) = \frac{s}{2\pi},$$

where $s$ is the intensity of the process. In Figure 15 the dependencies $\sigma_{uu,ww}(t)$ are depicted for $s = 5.3 \times 10^7$ N$^2$/s. Figures 15(a) and 15(b) are related to $V = 30$ and 75 m/s respectively. The solid lines in the figures reflect the variance of the vertical displacement, while the dashed line of the horizontal.

Figure 15(a) shows that for the sub-critical velocity the variance is a non-oscillatory function of time. Since the load is moving, this function is visibly asymmetric with respect to $t = 0$. However, the scale of this asymmetry in the sub-critical motion is incomparably smaller than that in the super-critical case, which is depicted in Figures 15(b). In the latter case, the variance at $t > 0$ is much larger than at $t < 0$. This is again due to the Doppler effect, providing that the observation point vibrates with lower frequencies and larger amplitudes at $t > 0$, when the load moves outwards this point (see Figure 7 and Figure 23 and associated explanations belonging to them). One can further see from Figure 15 that the variance in the super-critical motion is smaller that that in the sub-critical motion. This is because the super-critically moving load radiates waves with higher frequencies, which are stronger affected by the damping in the layer.

For practical requirements, it is important to known how the variance is related to the displacement provided by the gravity force. To visualize this relation, functions $u_0(t) \pm \sigma_{uu}(t)$ and $w_0(t) \pm \sigma_{ww}(t)$, are plotted in Figures 16 and 17 ($u_0(t)$ and $w_0(t)$ are the horizontal and the vertical displacements of the observation point under the constant load,

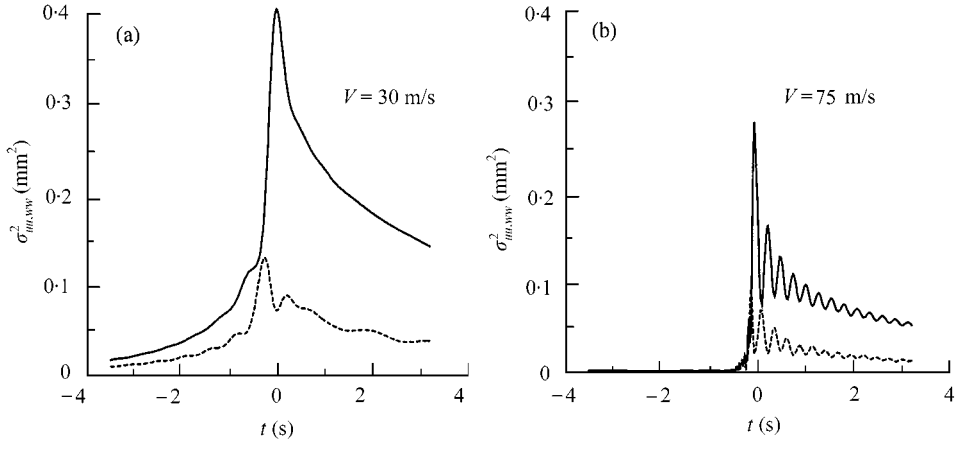


Figure 15. Variance of the displacements $u(0, 0, t)$ (dashed lines) and $w(0, 0, t)$ (solid lines) versus time.

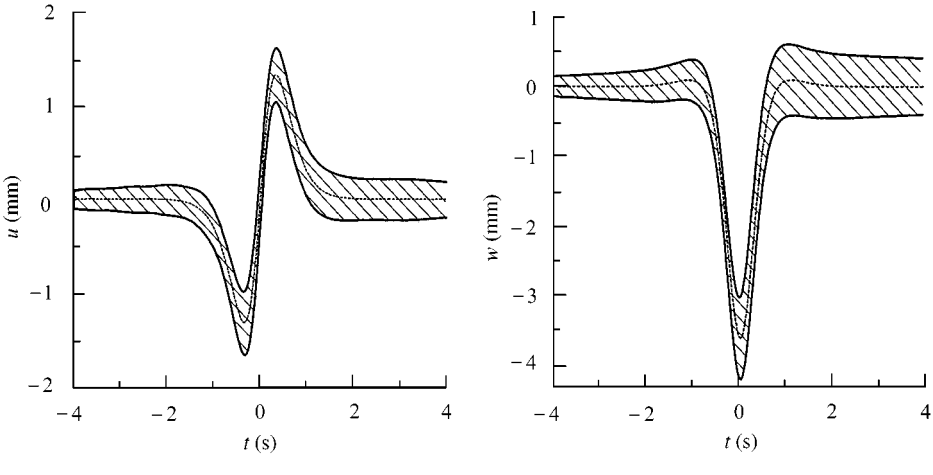


Figure 16. Domains of possible deviation of the displacements for $V = 30$ m/s.

which has been considered in section 5). The functions $u_0(t) \pm \sigma_{uu}(t)$ and $w_0(t) \pm \sigma_{ww}(t)$ are depicted by the solid lines and the functions $u_0(t)$ and $w_0(t)$ by the dashed lines. The shaded area indicates possible deviation of the displacements under the load $P_0 + P(t)$, where $P_0/a = 10\,\mathrm{kN/m}$ and $P(t)$ is the white noise with zero mean value and the intensity $s = 5.3 \times 10^7\ \mathrm{N^2/s}$.

Figures 16 and 17 clearly show that the deviation domains in the sub-critical case are much wider than that in the super-critical case. In the latter case, these domains are almost invisible. This implies that for the chosen parameters the statistical analysis is worth accomplishing only for the sub-critically moving load. The response in the super-critical motion can be accurately found by considering just the constant load.

## 8. CONCLUSIONS

The vibration response of a ground surface to a load moving in a tunnel has been investigated. The ground and the tunnel have been modelled by a two-dimensional elastic

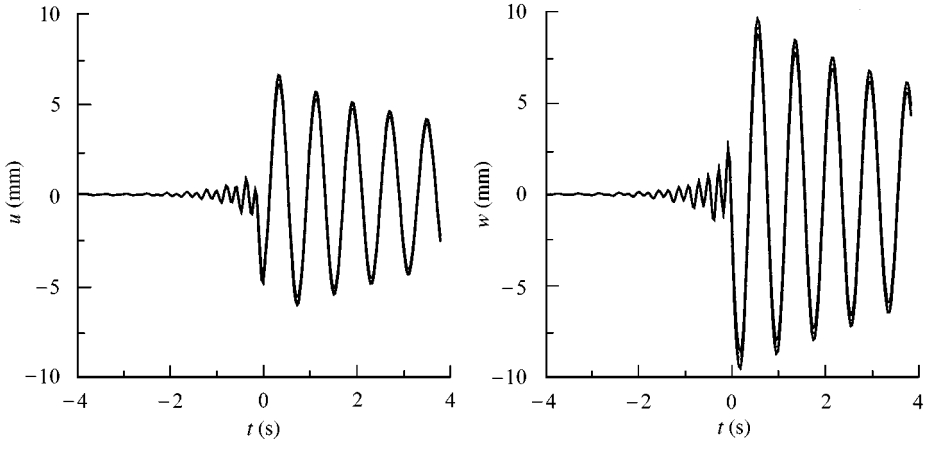


Figure 17. Domains of possible variation of the displacements for $V = 75$ m/s.

layer and an Euler–Bernoulli beam, respectively. The load has been considered point-like, vertical and moving uniformly along the beam.

First, the wave propagation in the structure has been studied. It has been shown that the only waves having the phase velocity smaller than the shear wave velocity $c_T$ in the layer may propagate along the structure with no attenuation. The amplitude of waves always decays if their phase velocity exceeds $c_T$. It has been demonstrated that the minimal phase velocity in the structure is smaller than the Rayleigh wave velocity in the layer and increases with the tunnel depth.

Based on the information about the wave dispersion in the structure, the response of the layer surface to three different types of the load has been analyzed. Namely, constant, a harmonically varying and a random stationary load have been considered. In the case of deterministic loads, the displacement and the amplitude spectra of an observation point on the surface have been studied. Considering the random load, main attention has been paid to the variance of vibrations in the observation point.

In the case of the constant load it has been shown that the structural response crucially depends on the ratio of the load velocity $V$ and the minimal phase velocity $V_{ph}^{min}$ of waves in the structure. In the sub-critical motion $V < V_{ph}^{min}$, the displacement of the observation point is pulse-like and the spectrum is concentrated around zero frequency having no peaks. On the contrary, in the super-critical motion ($V > V_{ph}^{min}$) the displacement pattern becomes wave-like and the spectrum possesses maxima caused by waves radiated by the load. The frequencies of these waves have been discussed by employing the kinematic analysis of the wave radiation in the structure. It has been shown that when the load velocity becomes close to $V_{ph}^{min}$, the amplitude of the structural response grows significantly.

In the case of the harmonically varying load, the surface response becomes wave-like at a substantially smaller load velocity than in the case of the constant load. Moreover, if the load frequency exceeds the cut-off frequency of the structure, waves are always excited, indifferently to whether the load moves or remains in a fixed position. Since for the chosen parameters, the cut-off frequency is very low (about 1 Hz), the only wave-like structural response has been analyzed. It has been shown that the spectrum of vibrations becomes more complicated and expands towards higher frequencies when the loading frequency grows.

Main attention in the case of the random load has been paid to the variance of vibration in the observation point. It has been shown that despite the stationary character of the load,

vibrations of the observation point are always non-stationary and, accordingly, the variance depends on time. This is due to the relative motion of the load with respect to the observation point. The level of the non-stationarity is strongly affected by the load velocity. The higher the load velocity, the higher the level of the non-stationarity. The standard deviation from the response to constant load has been evaluated showing significant dependence on the ratio $V/V_{ph}^{min}$. In the sub-critical motion this deviation is perceptible, while in the super-critical motion it appears to be very small. This implies that the response in the super-critical motion is much more deterministic than that in the sub-critical motion.

Concluding, one has to note that the two-dimensional model for a train moving in a tunnel is quite far from reality. Results obtained by studying this model can be treated only as an upper estimate of possible level of the ground vibration. To obtain more realistic results, one has to consider a three-dimensional model. For example, the ground can be modelled as a 3D elastic layer and the tunnel as a cylindrical shell.

## REFERENCES


1. P. NELSON 1987 *Transportation Noise Reference Book*. London: Butterworths.
2. V. V. KRYLOV 1995 *Applied Acoustics* **44**, 149–164. Generation of ground vibration by superfast trains.
3. H. A. DIETERMAN and A. METRIKINE 1997 *Transaction of the ASME Journal of Applied Mechanics*, **64**, 596–600. Critical velocities of a harmonic load moving uniformly along an elastic layer.
4. C. MADSHUS and A. KAYNIA 1998 *Proceedings of the 6th International Workshop on Railway Noise, Île des Embiez, France*, 108–119. High speed railway lines on the soft ground: dynamic behavior at critical train speeds.
5. D. V. JONES, D. LE HOUEDEC, A. T. PEPLOW and M. PETYL 1998 *European Journal of Mechanics A/Solids* **17**, 153–166. Ground vibration in the vicinity of a moving harmonic rectangular load.
6. H. A. DIETERMAN and A. METRIKINE 1996 *European Journal of Mechanics A/Solids* **15**, 67–90. The equivalent stiffness of a half-space interacting with a beam. Critical velocities of a moving load along the beam.
7. A. S. J. SUIKER, R. DE BORST and C. ESVELD 1998 *Archives of Applied Mechanics* **68**, 158–168. Critical behaviour of a Timoshenko beam - half plane system under a moving load.
8. H. KOLSKY 1963 *Stress Waves in Solids*. New York: Dover Publications, Inc.
9. G. A. KORN and T. M. KORN 1961 *Mathematical Handbook for Scientists and Engineers*, New York, McGraw-Hill.
10. J. T. KENNEY 1954 *Transactions of the ASME Journal of Applied Mechanics* **76**, 359–364. Steady-state vibrations of beam on elastic foundation for moving load.
11. J. D. ACHENBACH and C. T. SUN 1965 *International Journal of Solid and Structures* **1,** 353–370. Moving load on a flexible supported Timoshenko beam.
12. R. BOGACZ, T. KRZYZINSKI and K. POPP 1990 *ZAMM* **70**, T202–T203. On the group-phase velocities relations for continuous systems under moving loads.
13. A. I. VESNITSKII 1991 *Wave Dynamics of Machines* (K. V. Frolow, editor) 15–30. Moscow: Nauka. Wave effects in elastic systems (in Russian).
14. V. V. BOLOTIN 1984 *Random Vibrations of Elastic Systems*, The Hague, Martinus Nijhoff.


## APPENDIX A

The Fourier displacements $\tilde{\tilde{u}}$, $\tilde{\tilde{w}}$ and the Fourier stresses $\tilde{\tilde{\sigma}}_{zz}$, $\tilde{\tilde{\sigma}}_{xz}$ are expressed via the constants $A_j$, $j = 1, \ldots, 8$ as

$$\tilde{\tilde{u}} = ik(A_{1+n}\exp(zR_L) + A_{2+n}\exp(-zR_L)) + R_T(A_{3+n}\exp(zR_T) - A_{4+n}\exp(-zR_T)),$$

$$\tilde{\tilde{w}} = R_L(A_{1+n}\exp(zR_L) - A_{2+n}\exp(-zR_L)) - ik(A_{3+n}\exp(zR_T) - A_{4+n}\exp(-zR_T)),$$

$$\tilde{\tilde{\sigma}}_{zz} = (\mu - \mathrm{i}\omega\mu^*)\{(2k^2 - \omega^2/(c_T^2 - \mathrm{i}\omega\mu^*/\rho))(A_{1+n}\exp(zR_L) + A_{2+n}\exp(-zR_L))$$
$$- 2\mathrm{i}kR_T(A_{3+n}\exp(zR_T) - A_{4+n}\exp(-zR_T))\},$$
$$\tilde{\tilde{\sigma}}_{xz} = (\mu - \mathrm{i}\omega\mu^*)\{2\mathrm{i}kR_L(A_{1+n}\exp(zR_L) + A_{2+n}\exp(-zR_L))$$
$$+ (2k^2 - \omega^2/(c_T^2 - \mathrm{i}\omega\mu^*/\rho))(A_{3+n}\exp(zR_T) - A_{4+n}\exp(-zR_T))\}, \tag{A1}$$

when $n = 0$ for $z \in [0, h-0]$ and $n = 4$ for $z \in [h+0, h+H]$.

Expressions for $a_{ij}$ and $F_i$ in equation (19) read

$$a_{1j} = \left[ g_1(DR_L - \gamma), -\frac{DR_L + \gamma}{g_1}, \mathrm{i}kg_2(2R_T - D), -\frac{\mathrm{i}k(2R_T + D)}{g_2}, \gamma g_1, \frac{\gamma}{g_1}, -2\mathrm{i}kR_T g_2, \frac{2\mathrm{i}kR_T}{g_2} \right],$$

$$a_{2j} = [R_L g_1, -R_L/g_1, -\mathrm{i}kg_2, -\mathrm{i}k/g_2, -R_L g_1, R_L/g_1, \mathrm{i}kg_2, \mathrm{i}k/g_2],$$

$$a_{3j} = [\mathrm{i}kg_1, \mathrm{i}k/g_1, R_T g_2, -R_T/g_2, 0, 0, 0, 0],$$

$$a_{4j} = [0, 0, 0, 0, \mathrm{i}kg_1, \mathrm{i}k/g_1, R_T g_2, -R_T/g_2],$$

$$a_{5j} = [\gamma, \gamma, -2\mathrm{i}kR_T, 2\mathrm{i}kR_T, 0, 0, 0, 0],$$

$$a_{6j} = [2\mathrm{i}kR_L, -2\mathrm{i}kR_L, \gamma, \gamma, 0, 0, 0, 0],$$

$$a_{7j} = [0, 0, 0, 0, \mathrm{i}kg_3, \mathrm{i}k/g_3, R_T g_4, -R_T/g_4],$$

$$a_{8j} = [0, 0, 0, 0, R_L g_3, -R_L/g_3, -\mathrm{i}kg_4, -\mathrm{i}k/g_4],$$

$$F = [1/(a(\mu - \mathrm{i}\omega\mu^*)), 0, 0, 0, 0, 0, 0, 0],$$

where the following notations are introduced:

$$g_{1,2} = \exp(hR_{L,T}), \quad g_{3,4} = \exp((h+H)\,R_{L,T}), \quad \gamma = 2k^2 - \omega^2/(c_T^2 - \mathrm{i}\omega\mu^*/\rho),$$
$$D = (EI\,k^4 - \rho_B\omega^2)/(a(\mu - \mathrm{i}\omega\mu^*)).$$

## APPENDIX B

Let us evaluate the expression for $R_{uu}(t, t+\tau)$. Substituting equation (38) into equation (39) one obtains

$$R_{uu}(t, t+\tau) = \frac{1}{8\pi^3}\int_{\varphi}\int_{-\infty}^{+\infty}\int_{-\infty}^{+\infty}\sum_{n=1}^{N}\sum_{j=1}^{N} F_n(\Omega_n)\,F_j^*(\Omega_k)\exp(\mathrm{i}(\varphi_n - \varphi_j))\,\tilde{\tilde{u}}_0(k, kV - \Omega_n)$$
$$\times \exp(-\mathrm{i}(kV - \Omega_n)t)\,\tilde{\tilde{u}}_0^*(k_1, k_1V - \Omega_j)\exp(\mathrm{i}(k_1V - \Omega_j)(t+\tau))\,\mathrm{d}k\mathrm{d}k_1\,\mathrm{d}\boldsymbol{\varphi} \tag{B1}$$

Integration of equation (B1) with respect to $\boldsymbol{\varphi}$ yields

$$R_{uu}(t, t+\tau) = \frac{1}{4\pi^3}\int_{-\infty}^{+\infty}\int_{-\infty}^{+\infty}\sum_{n=1}^{N}\sum_{j=1}^{N} F_n(\Omega_n)\,F_j^*(\Omega_k)\,\tilde{\tilde{u}}_0(k, kV - \Omega_n)\exp(-\mathrm{i}(kV - \Omega_n)t)$$
$$\times \tilde{\tilde{u}}_0^*(k_1, k_1V - \Omega_j)\exp(\mathrm{i}(k_1V - \Omega_j)(t+\tau))\,\mathrm{d}k\mathrm{d}k_1, \tag{B2}$$

where $\delta_{jn} = \begin{cases} 1, & \text{when } n = j, \\ 0, & \text{when } n \neq j \end{cases}$

is the Kroneker's delta, which allows to reduce equation (41) to

$$R_{uu}(t, t+\tau) = \frac{1}{4\pi^3} \int_{-\infty}^{+\infty} \int_{-\infty}^{+\infty} \sum_{n=1}^{N} F_n(\Omega_n)\, F_n^*(\Omega_k)\, \tilde{\tilde{u}}_0(k, kV - \Omega_n) \exp(-\mathrm{i}(kV - \Omega_n)\, t)$$

$$\times \tilde{\tilde{u}}_0^*(k_1, k_1 V - \Omega_n) \exp(\mathrm{i}(k_1 V - \Omega_n)(t+\tau))\, \mathrm{d}k \mathrm{d}k_1$$

$$= \frac{1}{4\pi^2} \int_{-\infty}^{+\infty} \int_{-\infty}^{+\infty} \sum_{n=1}^{N} F_n(\Omega_n)\, F_n^*(\Omega_k)\, \tilde{\tilde{u}}_0(k, kV - \Omega_n) \exp(-\mathrm{i}Vt(k - k_1))$$

$$\times \tilde{\tilde{u}}_0^*(k_1, k_1 V - \Omega_n) \exp(\mathrm{i}(k_1 V - \Omega_n)\tau)\, \mathrm{d}k \mathrm{d}k_1.$$